Energy Conversion and Management 123 (2016) 453–461

Contents lists available at ScienceDirect

Energy Conversion and Management

journal homepage: www.elsevier.com/locate/enconman

Exergetic and energetic comparison of LiCl-H_2O and LiBr-H_2O working pairs in a solar absorption cooling system

Evangelos Bellos *, Christos Tzivanidis, Kimon A. Antonopoulos

Department of Thermal Engineering, National Technical University of Athens, Zografou, Heroon Polytechniou 9, 15780 Athens, Greece

ARTICLE INFO

Article history:
Received 1 May 2016
Received in revised form 20 June 2016
Accepted 26 June 2016
Available online 30 June 2016

Keywords:
Solar cooling
Absorption chiller
LiCl-H_2O
LiBr-H_2O
Exergy analysis

ABSTRACT

The objective of this study is to investigate the use of an alternative working pair in a solar absorption cooling system. LiCl-H_2O is the new examined pair and it is compared energetically and exegetically with the conventional pair LiBr-H_2O, which is the most usual in air-conditioning applications. The simplest solar cooling system is analyzed in order to focus in the comparison between these working fluids. Specifically, flat plate collectors, coupled with a storage tank, feed the single effect absorption chiller which produces 250 kW cooling at 10 °C. The two pairs are examined parametrically for various heat source temperature levels and for three ambient temperature levels (25 °C, 30 °C and 35 °C). The minimization of the collecting area, which means maximum exergetic efficiency, is the optimization goal in every case. The final results show that LiCl-H_2O pair performs better in all cases by giving greater exergetic efficiency. More specifically, about 8% lower collecting area is required to cover the demanded cooling load with this working pair. Another interesting result is that the optimum heat source temperature for the LiCl-H_2O is roughly lower than the respective for the LiBr-H_2O. The system is analyzed in steady state with the commercial software Engineering Equator Solver (EES).

1. Introduction

The new lifestyle trends lead our society to consume larger amounts of energy in order to achieve high standards of living. The fossil fuel depletion, the high cost of electricity and the environmental threats due to CO_2 emissions are the obstacles for reaching the desired energy consumption levels. Utilization of clean and sustainable energy sources is the most promising way to produce clean energy with zero CO_2 footprints [1,2]. Solar energy is the most abundant and widespread renewable energy source and it is able to give solutions in many applications with high energy demand. Energy consumption in building sector is approximately 35% of the global energy consumption and its greatest part is responsible for covering heating and cooling loads [3]. Moreover, the new lifestyle increases the energy consumption by the progressively changing thermal comfort standards [4]. Two practices have applied in order to face this crucial situation. The first one is the optimization of the building cell [5,6] in order to reduce the energy demand on cooling and heating loads. The second way is to exploit renewable energy sources, mainly solar energy, for covering a great part of the loads.

Solar cooling is a very promising technology that is able to cover the cooling load by utilizing the solar energy. Three are the main technologies for applying solar cooling; absorption chillers, absorption chillers and desiccant systems with the first to be the most used worldwide [7]. Various collector types are able to be combined with these chillers in order to produce the demanded cooling load. Flat plate collectors (FPC), which are the cheapest and more mature technology [8], can be used for producing useful heat in temperature levels up to 100 °C. For greater temperature levels, evacuated tube collectors [9] are usually used, while concentrating collectors are also a reliable solution [10].

In the absorption chillers, two are the usual refrigerant-absorbent working pairs, with NH_3-H_2O to be used for refrigeration temperatures under 0 °C and H_2O-LiBr for higher refrigeration temperature levels. Moreover, other working pairs can be used, instead H_2O-LiBr, as lithium chloride/water (LiCl-H_2O), ammonia-sodium thiocyanate (NH_3-NaSCN) and ammonia/calcium chloride (NH_3-$CaCl_2$) [7]. According to many researches, the use of LiCl-H_2O in absorption cycle gives satisfying results compared to LiBr-H_2O pair [11,12]. Parham et al. [13] stated that the exergetic efficiency of absorption cycle with LiCl-H_2O is higher than the respective with LiBr-H_2O. She et al. [14], after a detailed analysis proved that LiCl-H_2O performs better than LiBr-H_2O in all operating conditions. Moreover, LiCl-H_2O has greater long-term stability [13] and has

* Corresponding author.
E-mail address: bellose@central.ntua.gr (E. Bellos).

http://dx.doi.org/10.1016/j.enconman.2016.06.068
0196-8904/

Nomenclature

A	area (m^2)
D	diameter (m)
E	exergy flow (kW)
G_T	solar radiation (W/m^2)
h	enthalpy (kJ/kg)
L	height (m)
m	mass flow rate (kg/s)
M	the storage water mass (kg)
P	pressure (kPa)
Q	heat rate (W)
SCOP	solar coefficient of performance
t	time (s)
T	temperature (K)
U_L	tank heat loss coefficient (W/m^2)
V_T	tank volume (m^3)
X	LiBr mass concentration in mixture

Greek symbols

η	efficiency
ρ_f	water density (kg/m^3)

Subscripts and superscripts

A	absorber
am	ambient
C	condenser
chill	chiller
col	collector
E	evaporator
ex	exergy
HEX	heat exchanger
in	inlet
G	generator
loss	heat losses
out	outlet
r	refrigerant
S	heat source
sol	solar energy
st1	1st zone of the storage tank
st2	2nd zone of the storage tank
st3	3rd zone of the storage tank
Str	strong solution
sun	sun
T	titled
th	thermal
U	useful
w	weak solution

Abbreviations

COP	coefficient of performance
EES	Engineer Equator Solver
FPC	flat plate collector
LiBr	lithium bromide
LiCl	lithium chloride
SCOP	solar coefficient of performance

great internal energy storage capacity [11], two important reasons for selecting this working pair in an absorption refrigeration chiller. Sahem et al. [15] investigated parametrically the performance of LiCl-H_2O in various operating conditions and proved that the maximum COP is close to 0.8. Furthermore, they stated that the maximum accepted temperature of the cooling medium has not to exceed 40 °C. Beausoleil-Morrison et al. [16] studied a Small-scale solar air conditioning system operating with LiCl-H_2O and proved that when the generator temperature is ranged from 71 °C to 93 °C, the COP varies from 0.53 to 0.83.

This study aims to compare the working couple LiCl-H_2O with the usual couple LiBr-H_2O in solar cooling applications, something that is not well-established up today. This study is innovative because the comparison is parametrically for various values of ambient temperature and heat source temperature, something that is missing from the literature. In every case, the optimized system is determined in order to minimize the demanded collecting area for producing the desired cooling load. The systems are examined energetically and exegetically in order to present a more detailed analysis. The optimization parameter is the heat source temperature, the temperature of hot water in the generator inlet, a methodology that has been also followed in many studies [15,17,18]. The suitable selection of heat source temperature maximizes the exergetic efficiency of the system and minimizes the demanded solar field area. The simulation is made for steady state conditions with commercial software EES (Engineer Solver Equator), in order to focus on the comparison between the two working pairs. The properties of each working fluid are taken from EES database. More specifically, for LiCl-H_2O the properties are taken from Patek and Klomfar study [19] which is on accordance with a newer study of Li et al. [20].

2. Study case

2.1. System description and assumptions

A solar cooling system is analyzed in steady state conditions in order to focus in the comparison between the examined working pairs. Simultaneously, the system operation is optimized in order to evaluate every working pair in the suitable operating conditions. The main parts of the examined system are the solar collector field, the storage tank and the absorption chiller. These parts are coupled to each other according to Fig. 1. More specifically, solar energy is captured by flat plate collectors and the working fluid is getting warmer. The working fluid is pressurized water in order to remain in liquid phase during the process. The hot water from the collector field outlet is stored in a storage tank. This storage tank is modelled with mixing zones and loss heat into the environment (Q_{loss}). This tank has two inlets and two outlets, according to Fig. 1. The hot water from the collectors has temperature $T_{c,out}$ and enters in the upper part of tank. From the lower part of the tank, water with temperature $T_{c,in}$ leaves it and enters to the collector field. On the other side of the tank, hot water from its upper part with temperature $T_{s,in}$ goes to the generator of the absorption chiller. This temperature level is characteristic for this study and will be referred as heat source temperature. The return stream from the chiller has temperature $T_{s,out}$ and enters in the lower part of the tank.

The absorption chiller is a single effect chiller with heat exchanger and operates with LiBr-H_2O or LiCl-H_2O. Solar energy is the input energy into generator and the energy input in the evaporator is the cooling load of this system. Heat rejection to the environment takes place in the condenser and in the absorber. In order to simulate this system, some assumptions have been made. These

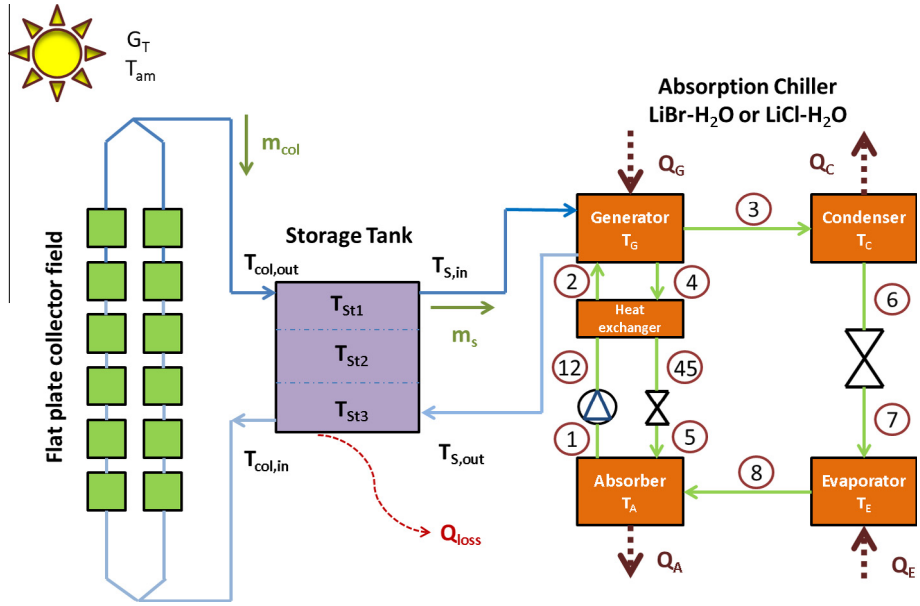

Fig. 1. Solar cooling system (solar field, storage tank and absorption chiller).

assumptions are usual to solar absorption systems and have been used in many other studies [18,21,22]. The following Eqs. (1)–(3) present the assumptions for the temperature differences between the different streams. More specifically, the generator temperature is set to be 10 K lower than the heat source temperature ($T_{s,in}$), according to the Eq. (1):

$$T_G = T_{s,in} - 10, \quad (1)$$

The hot stream after the generator has a temperature drop of about 7 K, according to Eq. (2):

$$T_{s,out} = T_{s,in} - 7, \quad (2)$$

Absorber and condenser reject heat to the ambient and for this reason these devices operate at same temperature level. Eq. (3) shows that the heat rejection temperature is 10 K greater than the ambient temperature.

$$T_C = T_A = T_{am} + 10, \quad (3)$$

Three different ambient temperature levels are investigated (25 °C, 30 °C and 35 °C); a strategy which examines the system in the usual temperature levels for the summer period. In the simulation, many parameters have been kept constant for all study cases. More specifically, the cooling load is 250 kW and the evaporating temperature 10 °C. The heat exchanger efficiency is set to be 70% [21], a realistic value for usual absorption chillers. The heat loss coefficient from the tank to the environment is selected to be 0.5 W/m^2 K [18], which means an insulated tank. This heat loss coefficient includes convection and radiation losses.

Other parameters are calculated according to usual formulas. The storage tank volume is calculated by Eq. (4) [17], while mass flow rates in the solar field circuit and in the heat source circuit according to Eqs. (5) and (6) [18,23]:

$$V_T = \frac{A_C}{30}, \quad (4)$$

$$\dot{m}_{col} = 0.02 \cdot A_{col}, \quad (5)$$

$$m_s = m_{col}, \quad (6)$$

3. Mathematical definitions and modelling

In the mathematical modelling of this study, many equations have been used in order to present the system behavior. The majority of these equations have been described in our previous work in Ref. [18] and for this reason only the basic equations are given below.

3.1. Solar field calculations

In this section, the main equations which describe this problem are given. Theses equations are related to the efficiency of the system which is presented by various ways. First of all the equations about the solar collector field are given.

The available solar energy is calculated by the incident solar energy G_T and the collector area A_c, according to Eq. (7):

$$Q_{sol} = A_{col} \cdot G_T, \quad (7)$$

The useful heat of the solar collector Q_u can be calculated by the energy balance in the working fluid volume. Eq. (8) shows the way that this quantity is calculated:

$$Q_u = \dot{m}_{col} \cdot c_p \cdot (T_{col,out} - T_{col,in}), \quad (8)$$

By combining this energy flow streams, the thermal efficiency of the collector $\eta_{th,col}$ is calculated by Eq. (9):

$$\eta_{th,col} = \frac{Q_u}{Q_{sol}}, \quad (9)$$

In this study, a typical selective flat plate collector is used for capturing the solar energy. The equation which describes its performance is given below [24]:

$$\eta_{th,col} = 0.75 - 5.0 \cdot \left(\frac{T_{col,in} - T_{am}}{G_T}\right), \quad (10)$$

3.2. Storage tank modelling

The mixing zone strategy is followed in the storage tank modelling. Every mixing zone is assumed to have a uniform temperature level and it exchanges mass and energy with the neighbor zones. In this study, three mixing zones are used, a strategy which lead to satisfying results. The energy balance in every mixing zone leads to a differential equation. Eqs. (11)–(14) are the three differential equations which describes the behavior of the storage tank.

$$\frac{M}{3}\cdot c_p\cdot\frac{\partial T_{St1}}{\partial t}=\dot{m}_{col}\cdot cp\cdot(T_{col,out}-T_{St1})+\dot{m}_s\cdot cp\cdot(T_{St2}-T_{St1})-U_L\cdot A_{St1}\cdot(T_{St1}-T_{am}),\quad(11)$$

$$\frac{M}{3}\cdot c_p\cdot\frac{\partial T_{St2}}{\partial t}=\dot{m}_{col}\cdot cp\cdot(T_{St1}-T_{St2})+\dot{m}_s\cdot cp\cdot(T_{St3}-T_{St2})-U_L\cdot A_{St2}\cdot(T_{St2}-T_{am}),\quad(12)$$

$$\frac{M}{3}\cdot c_p\cdot\frac{\partial T_{St3}}{\partial t}=\dot{m}_{col}\cdot cp\cdot(T_{St2}-T_{St3})+\dot{m}_s\cdot cp\cdot(T_{s,out}-T_{St3})-U_L\cdot A_{St3}\cdot(T_{St3}-T_{am}),\quad(13)$$

In this modelling the heat source temperature ($T_{s,in}$) is equal to the T_{St1} and the inlet temperature to the collectors ($T_{col,in}$) is equal to T_{St3}. The thermal losses of the storage tank are different from zone to zone because every zone has its own temperature and outer area. Eqs. (14)–(16) show the outer area of the three zones by assuming a cylindrical tank of diameter D_{St} and height L_{St}. In this study, these two parameters were selected to have the same values, an assumption with a very small impact on the final results.

$$A_{St1}=\frac{\pi\cdot D_{St}^2}{4}+\frac{\pi\cdot D_{St}\cdot L_{St}}{3},\quad(14)$$

$$A_{St2}=\frac{\pi\cdot D_{St}\cdot L_{St}}{3},\quad(15)$$

$$A_{St3}=\frac{\pi\cdot D_{St}^2}{4}+\frac{\pi\cdot D_{St}\cdot L_{St}}{3},\quad(16)$$

The water mass included in every zone is the one third of the total mass (M) in the storage tank, which is given by Eq. (17):

$$M=\rho_f\cdot V_T,\quad(17)$$

It is essential to state that water density (ρ_f) and heat capacity (cp) are calculated for the respective temperature levels and they are taken by EES libraries.

3.3. Absorption chiller modelling and exergetic calculations

The basic equations which describe the operation of the absorption chiller (Fig. 1) have been presented in Ref. [18]. The basic equations, which are related to the overall system performance, are given below.

The chiller performance is determined by the coefficient of performance (COP) which is defined as the ratio of the refrigeration to the heat input:

$$COP=\frac{Q_E}{Q_G},\quad(18)$$

The next useful parameter of the solar cooling system is the solar COP which takes into consideration the solar energy input and no the heat source input in the generator. Eq. (19) presents this parameter:

$$SCOP=\frac{Q_E}{Q_{sol}},\quad(19)$$

The exergetic analysis is based on two important indexes; the chiller exergetic performance and the solar system exergetic performance. The first is given from Eq. (20) and the second from Eq. (21) [25].

$$\eta_{ex,chill}=\frac{\left|Q_E\cdot\left(1-\frac{T_{am}}{T_E}\right)\right|}{Q_G\cdot\left(1-\frac{T_{am}}{T_G}\right)},\quad(20)$$

$$\eta_{ex,sol}=\frac{\left|Q_E\cdot\left(1-\frac{T_{am}}{T_E}\right)\right|}{A_c\cdot G_T\cdot\left[1-\frac{4}{3}\cdot\left(\frac{T_{am}}{T_{sun}}\right)+\frac{1}{3}\cdot\left(\frac{T_{am}}{T_{sun}}\right)^4\right]},\quad(21)$$

The sun temperature (T_{sun}) in the above equation is equal to 4350 K and is equal to the 75% of the sun temperature in its outer layer [23]. By maximizing the solar system exergetic efficiency, the examined system has optimum performance. More specifically, greater exergetic efficiency leads to lower collecting area in the solar field, something that is proved by the results of this study.

4. Methodology and validation

4.1. Methodology description

In this study, two different working pairs in the absorption chiller are tested in order to predict their performance. In this study, the demanded cooling load is kept constant and the goal is to predict the minimum collecting area that is able to produce this demanded cooling load. The most important parameter is the heat source temperature ($T_{s,in}$) which determines the system efficiency and a sensitivity analysis is made in order to predict the optimum value of this parameter. More specifically, a greater heat source temperature makes the absorption chiller to perform better by increasing its COP. On the other hand, a greater heat source temperature means hotter water in the collector circuit, something that leads to lower thermal efficiency of the solar field. For these reasons, an intermediate heat source temperature leads to optimum performance, according to the following results.

Fig. 2 illustrates the equations path of the followed methodology. It is important to state that the presented methodology is similar to the respective in Ref. [18], but here it is extended also for the working pair LiCl-H_2O.

4.2. Validation

In this paragraph, the validation of the chiller model is presented. The developed model in EES is compared with the results of Godoi and Konwar study [22], where LiCl-H_2O and LiBr-H_2O are examined and compared. In this study, the cooling load is equal to 350 kW and the heat exchanger effectiveness is 75%. Table 1 includes the validation results for the examined working pairs.

The comparison in Table 1 proves that the developed model is close to the literature model. More specifically, the mean difference for the LiBr-H_2O pair is 0.38%, while for the LiBr-H_2O is 1.44%. These small differences prove that the absorption chiller calculations are accepted and reliable.

5. Performance of system parts separately

5.1. Absorption chiller performance

The chiller performance is presented in this section by Figs. 3 and 4. In these figures the COP and the exergetic efficiency are given for various cases. More specifically, two different working pairs are examined, LiCl-H_2O and LiBr-H_2O, in order to predict the most efficient pair. Moreover, the system performance is analyzed for 3 different condensation temperatures in order to cover a great range of operating conditions. It is important to state the absorption temperature was set equal to condensation temperature. The COP and the exergetic efficiency are presented as a function of generator temperature in Figs. 3 and 4 respectively.

From Figs. 3 and 4 it is obvious that the pair LiCl-H_2O performs better than LiBr-H_2O for all the examined cases. Moreover, a greater condensation temperature leads to greater exegetic efficiency but to lower COP. The reason for this greater exergetic efficiency is the system operation in higher generator temperature levels. In this point, it essentially to state that the use of LiCl-H_2O

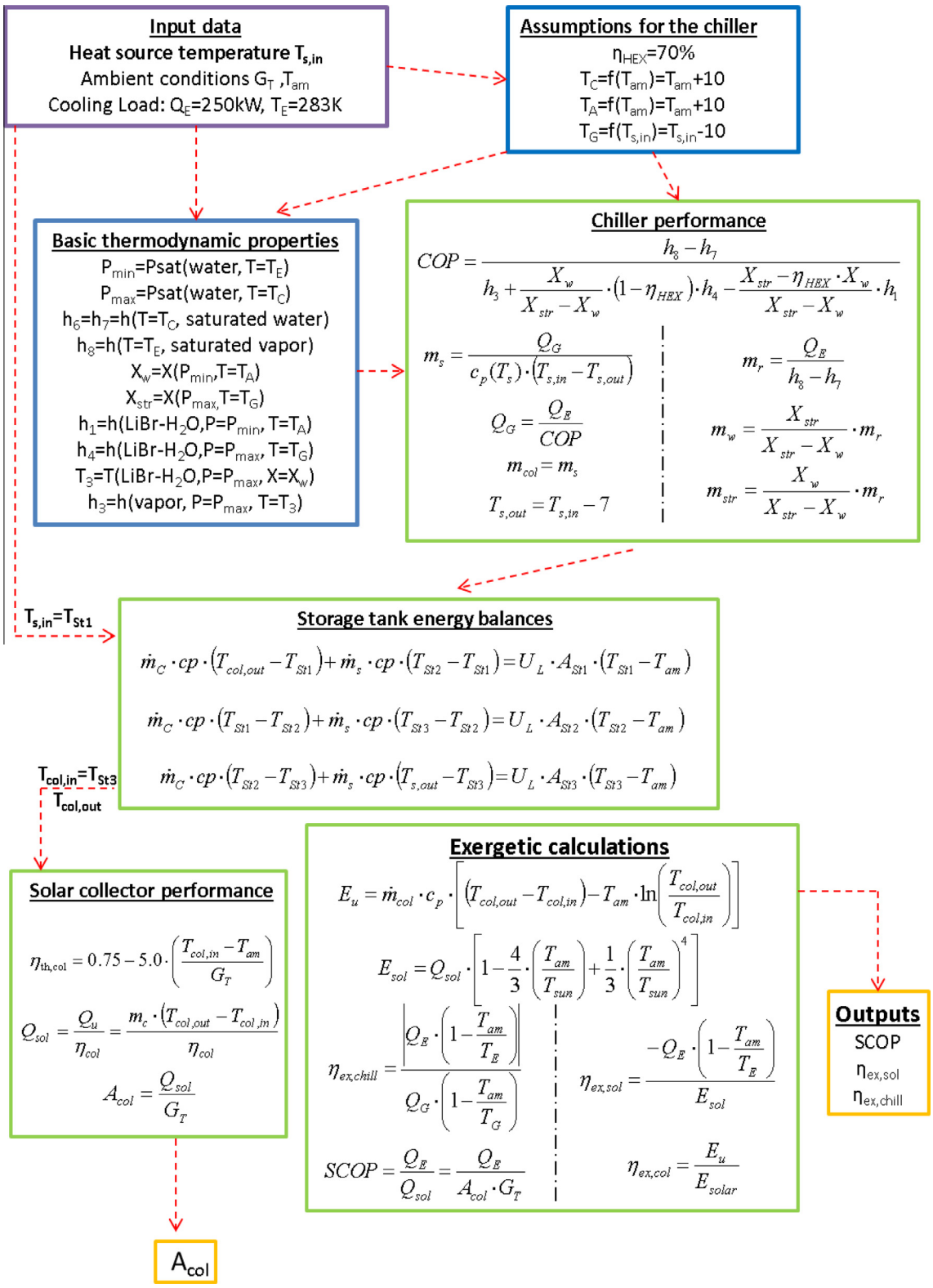

Fig. 2. Equations path of the present methodology.

creates constraints in the generator temperature range, something that is obvious from Figs. 3 and 4. The last important conclusions from these figures are the existence of maximum value in every exergetic curve for an intermediate generator temperature and the COP curves approximation to a maximum value while the generator temperature increases.

5.2. Flat plate collector performance

The solar field is consisted of flat plate collectors which are the most widespread collector type. In this study, high quality selective flat plate collectors are used in order to perform efficiently in temperature levels close to 100 °C. The working fluid is pressurized

Table 1
Validation results.

Examined cases				LiCL-H_2O			LiBr-H_2O		
T_E (°C)	T_G (°C)	T_C (°C)	T_A (°C)	COP Ref. [22]	COP This study	Difference (%)	COP Ref. [22]	COP This study	Difference (%)
4	70	31	31	0.855	0.869	1.64	0.794	0.790	0.50
4	69	31	35	0.842	0.834	0.95	0.697	0.702	0.72
5	66	28	35	0.856	0.841	1.75	0.769	0.766	0.39
6	72	33	37	0.839	0.842	0.36	0.730	0.729	0.14
8	63	25	37	0.872	0.889	1.95	0.819	0.817	0.24
8	85	46	39	0.807	0.792	1.86	0.585	0.589	0.68
9	66	28	34	0.877	0.891	1.60	0.837	0.837	0.00

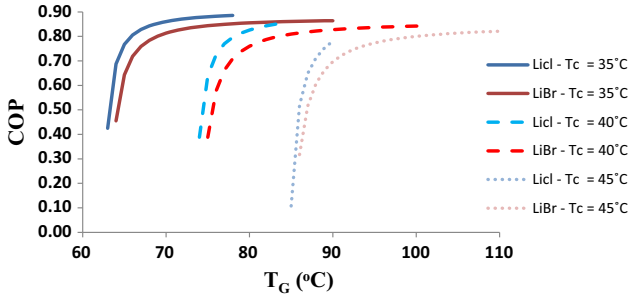

Fig. 3. Absorption chiller coefficient of performance (COP) for various condensation temperature levels (35 °C–40 °C–45 °C) and for the two working pairs.

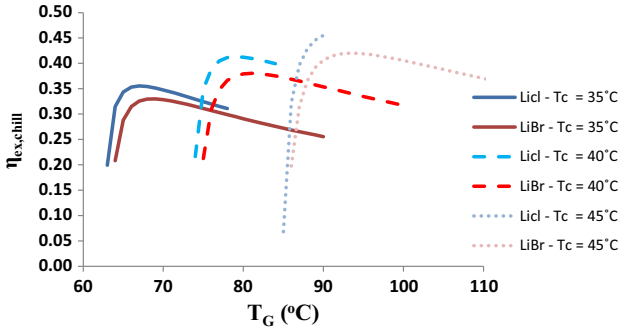

Fig. 4. Absorption chiller exergetic efficiency for various condensation temperature levels (35 °C–40 °C–45 °C) and for the two working pairs.

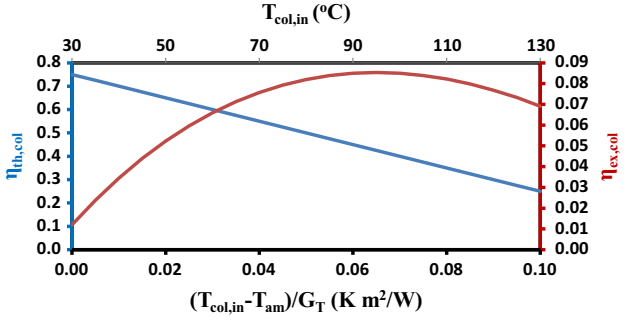

Fig. 5. Thermal and exergetic efficiency of the examined flat plate collector.

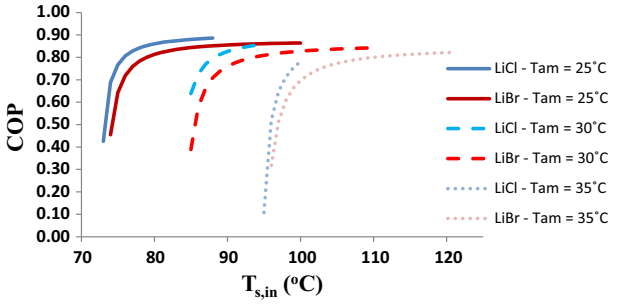

Fig. 6. Heat source temperature impact on the COP for various ambient temperature levels (25 °C–30 °C–35 °C) and for the two working pairs.

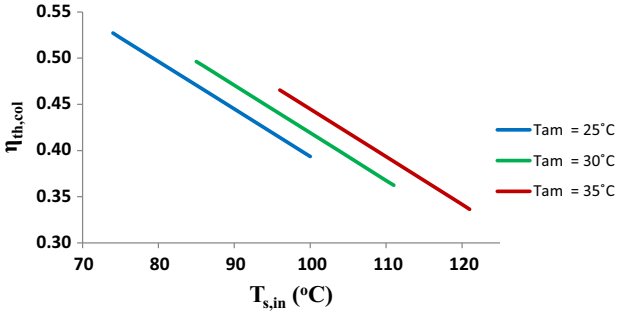

Fig. 7. Heat source temperature impact on the FPC thermal efficiency for various ambient temperature levels (25 °C–30 °C–35 °C).

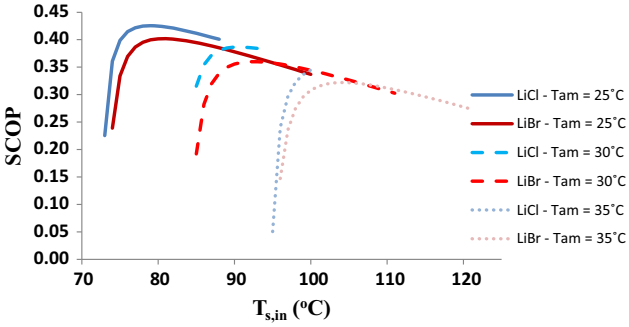

Fig. 8. Heat source temperature impact on the solar COP for various ambient temperature levels (25 °C–30 °C–35 °C) and for the two working pairs.

water which is kept in liquid phase in all the examined cases. Fig. 5 depicts the thermal and the exergetic efficiency of the selected flat plate collector.

The thermal efficiency is a linear function of quantity $(T_{col,in} - T_{am})/G_T$ while the exergetic efficiency curve has a parabolic shape. Interesting is the existence of maximum exergetic efficiency for inlet temperature equal to 90 °C. This result predicts the operation region of the collector for exergetic optimum performance. In a solar cooling system, the region from 90 to 100 °C, is ideal and for this reason the examined collector is suitable for the present study case.

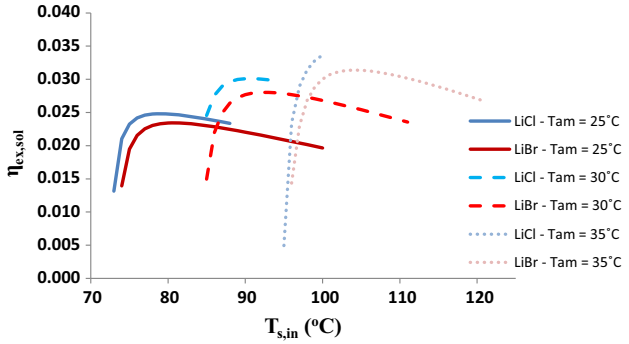

Fig. 9. Heat source temperature impact on the solar exergetic efficiency for various ambient temperature levels (25 °C–30 °C–35 °C) and for the two working pairs.

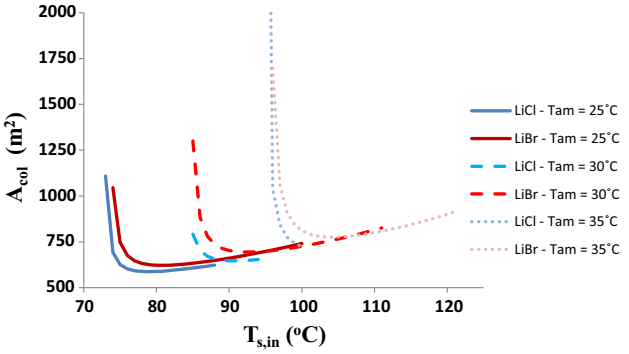

Fig. 10. Heat source temperature impact on the collecting area for various ambient temperature levels (25 °C–30 °C–35 °C) and for the two working pairs.

6. Results of the simulation

6.1. Performance of the solar cooling system for various cases

The solar cooling system was examined for various cases in order to determine the optimum operating conditions. More specifically Figs. 6–9 show the main results of the analysis. In every figure there are 6 curves, separated to 3 pairs, each pair for different ambient temperature level (25 °C–30 °C–35 °C). The system performance is investigated for operating with LiCl-H_2O and LiBr-H_2O parametrically with the heat source temperature. A general result is that lower ambient temperature level demands lower heat source temperature for normal operation. This can be explained by taking into consideration the danger of crystallization in high condensation temperature levels. Fig. 6 depicts the coefficient of performance for all the examined cases. There are 3 couples of curves and every couple is consisted of a curve for LiBr-H_2O and one for LiCl-H_2O. The second working pair, which is the alternative one, performs better to all the cases and makes the chiller efficiency higher. The higher ambient temperature, which corresponds to higher condensation and absorption temperature level, leads to lower COP. Every curve increases with the increase of heat source temperature, an accepted and logical. However, it is interesting that after a point, different for every curve, this increase is lower and each curve moves towards asymptotically to its maximum COP value. Another interesting result is that the range of the accepted heat source temperature level is smaller in the case of LiCl-H_2O, because of restriction which is related to crystallization danger. Fig. 7 depicts the thermal collector efficiency as a function of the heat source temperature levels. The most important results from this figure, which has similarities with Fig. 6, are that the thermal efficiency of the collectors is getting greater for higher ambient temperature levels and getting lower for higher heat source temperature levels.

Table 2
Properties of points, for optimum cases with LiBr-H_2O.

Points	T_{am} = 25 °C				T_{am} = 30 °C				T_{am} = 35 °C			
	T (°C)	h (kJ/kg)	P (kPa)	X (–)	T (°C)	h (kJ/kg)	P (kPa)	X (–)	T (°C)	h (kJ/kg)	P (kPa)	X (–)
1	35.0	76	1.23	0.561	40.0	94	1.23	0.590	45.0	114	1.23	0.600
12	35.0	76	5.63	0.561	40.0	94	7.38	0.590	45.0	114	9.59	0.600
2	61.0	132	5.63	0.561	72.1	160	7.38	0.590	79.1	182	9.59	0.600
3	63.3	2618	5.63	–	74.2	2638	7.38	–	85.3	2659	9.59	–
4	71.0	161	5.63	0.522	83.0	196	7.38	0.549	91.0	216	9.59	0.574
45	42.3	102	5.63	0.522	48.2	125	7.38	0.549	54.1	145	9.59	0.574
5	42.3	102	1.23	0.522	48.2	125	1.23	0.549	50.2	145	1.23	0.574
6	35.0	147	5.63	–	40.0	168	7.38	–	45.0	188	9.59	–
7	10.0	147	1.23	–	10.0	168	1.23	–	10.0	188	1.23	–
8	10.0	2519	1.23	–	10.0	2519	1.23	–	10.0	2519	1.23	–

Table 3
Properties of points, for optimum cases with LiCl-H_2O.

Points	T_{am} = 25°C				T_{am} = 30°C				T_{am} = 35°C			
	T (°C)	h (kJ/kg)	P (kPa)	X (–)	T (°C)	h (kJ/kg)	P (kPa)	X (–)	T (°C)	h (kJ/kg)	P (kPa)	X (–)
1	35.0	139	1.23	0.431	40.0	177	1.23	0.474	45.0	220	1.23	0.497
12	35.0	139	5.63	0.431	40.0	177	7.38	0.474	45.0	220	9.59	0.497
2	62.5	213	5.63	0.431	74.0	266	7.38	0.474	82.7	314	9.59	0.497
3	63.0	2617	5.63	–	75.0	2639	7.38	–	84.8	2658	9.59	–
4	69.0	257	5.63	0.385	81.0	319	7.38	0.423	91.0	367	9.59	0.462
45	40.9	174	5.63	0.385	46.5	220	7.38	0.423	50.1	264	9.59	0.462
5	40.9	174	1.23	0.385	46.5	220	1.23	0.423	50.1	264	1.23	0.462
6	35.0	147	5.63	–	40.0	168	7.38	–	45.0	188	9.59	–
7	10.0	147	1.23	–	10.0	188	1.23	–	10.0	188	1.23	–
8	10.0	2518	1.23	–	10.0	2519	1.23	–	10.0	2519	1.23	–

Table 4
Final results of all optimum cases.

Pairs	T_{am} (°C)	$T_{s,in}$ (°C)	V_T (m^3)	A_{col} (m^2)	$\eta_{ex,sol}$	SCOP	COP	$\eta_{th,col}$
LiCl-H_2O	25	79	19.6	587	0.0248	0.4256	0.8532	0.5014
	30	91	21.6	647	0.0301	0.3866	0.8357	0.4655
	35	101	23.0	689	0.0354	0.3628	0.8309	0.4398
LiBr-H_2O	25	81	20.7	622	0.0234	0.4018	0.8224	0.4912
	30	93	23.1	694	0.0280	0.3600	0.7959	0.4552
	35	104	25.9	776	0.0314	0.3220	0.7644	0.4243

Figs. 8 and 9 illustrate the solar COP and the exergetic efficiency of the system respectively. It is obvious that there are maximum points in all the curves which represent the optimum operating conditions. A low heat source temperature lead to low COP, according to Fig. 6, but to higher solar thermal efficiency according to Fig. 8. This inverse relationship between solar thermal efficiency and COP creates an optimum point in every curve of Fig. 9. Another important conclusion is that the SCOP is getting lower when the ambient temperature increases while the exergetic efficiency has the opposite behavior. These can be explained easily, by taking into consideration the impact of ambient temperature in the definition of every parameter. For SCOP, a greater ambient temperature increases the condensation temperature and the COP is getting lower, something that is proved in Fig. 6. The solar exergetic efficiency is influenced by thermal efficiency of the solar field and for this reason increases for higher ambient temperature levels.

In every case, the optimum solution is determined by the maximum points in the curves of Figs. 8 and 9. It is important to state that these maximum points are observed for the same heat source temperatures among the respective curves. The maximization of SCOP and $\eta_{ex,sol}$ lead to minimum solar collecting area, according to Fig. 10. The most important conclusion from Fig. 10 is that the solar field collecting area increases for higher ambient temperature levels. This means that the warmer climate has a negative impact on solar cooling technologies. More specifically, higher ambient temperature leads to higher condensation temperature, in order to reject the heat to the environment properly, something with a negative impact on the COP.

6.2. Comparison of optimum solutions and discussion

In the previous section the system performance for various cases was presented. Six different cases have been analyzed thus 6 optimum cases have been resulted. Tables 2 and 3 include the state points (1–8) of the absorption cycle for all these cases. More specifically, Table 2 includes the data for the working pair LiBr-H_2O and Table 3 for LiCl-H_2O. The points in these tables are determined in Fig. 1. A remarkable result is the lower concentrations (X) in the LiCl-H_2O case because of its higher crystallization danger. It is important to state that the maximum concentration in the LiCl-H_2O is about 0.5 while for LiBr-H_2O is 0.75 [22]. This observation proves difficulties in the design of an absorption chiller operating with LiCl-H_2O. Table 4 and Fig. 11 summarize

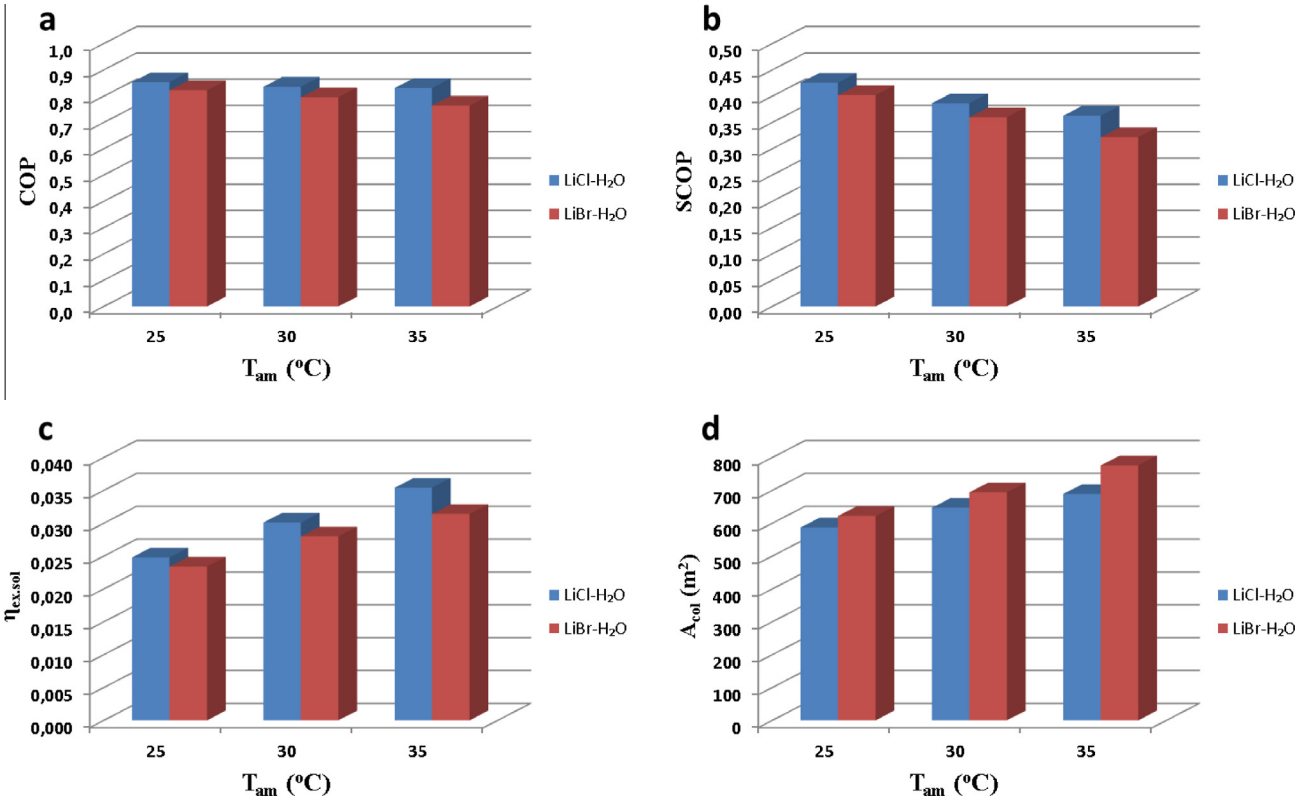

Fig. 11. Final comparisons between the two working pairs for the examined ambient temperature levels.

the study results, presenting the most important parameters of the six optimum cases. The comparison between the two working fluids is more obvious in Fig. 11.

The optimum working pair is LiCl-H_2O because lower collecting area is needed in its cases. All the performance indexes, as COP, SCOP and exergetic efficiencies, are greater in the LiCl-H_2O case, something that proves a clear energetic difference between the two examined working pairs. It is important to be stated the exergetic efficiency is low, about 0.02–0.03 because the evaporator temperature is close to the environmental. In all the examined cases between the two working pairs, lower heat source temperature is needed for LiCl-H_2O. This difference is small and it is about 2–3 K, but it renders the LiCl-H_2O as the most suitable working pair. Moreover, the lower optimum temperature leads to lower operation temperature in the system and in the collectors, fact that increases the thermal efficiency of the collector field. A general observation is that the low value of solar exergetic efficiency is explained by the low exergetic quality of cooling output. Moreover, it is important to state that the mean specific collecting area is 2.68 m^2/kW; a realistic value according to other studies [26].

7. Conclusions

A solar cooling system is analyzed and optimized energetically and exegetically. Two working pairs are investigated; the alternative LiCl-H_2O and the conventional LiBr-H_2O. The final results proved that LiCl-H_2O is better energetically and exergetically in all the examined cases. A simple optimization method is applied in order to determine the optimum heat source temperature for every working pair for three usual ambient temperature levels (25 °C–30 °C–35 °C). The optimization goal is the maximization of the system exergetic efficiency which corresponds to minimization of the demanded collecting area. This goal is equivalent as maximizing the SCOP or the solar exergetic efficiency of the system.

The final results show that about 8% lower collecting area is needed in the case of LiCl-H_2O. Also, the optimum heat source temperature is lower in the case of LiCl-H_2O which is an extra advantage of this working pair. These results prove that the alternative working pair LiCl-H_2O is beneficial compared to the conventional LiBr-H_2O. However, the crystallization danger is greater in the operation with LiCl-H_2O, something that has to be taken into account in the absorption chiller design.

Moreover, the system was analyzed for 3 different ambient temperature levels for covering a variety of environmental conditions. The influence of ambient temperature on the efficiency parameters is remarkable. COP and SCOP are diminished for greater ambient temperatures, while solar collector efficiency and solar exergetic efficiency takes higher values. The collecting area in the cases with higher ambient temperature is getting higher something that proves the negative impact of the high environment temperature. The final conclusion of this study is that the use of LiCl-H_2O as working pair in an absorption cycle performs better than LiBr-H_2O and the solar cooling system performs better in climates with lower mean ambient temperature.

Acknowledgments

The first author would like to thank the Onassis Foundation for its financial support.

References

[1] Zhang X, Li H, Liu L, Zeng R, Zhang G. Analysis of a feasible trigeneration system taking solar energy and biomass as co-feeds. Energy Convers Manage 2016;122:74–84.
[2] Bellos E, Tzivanidis C, Antonopoulos KA, Gkinis G. Thermal enhancement of solar parabolic trough collectors by using nanofluids and converging-diverging absorber tube. Renew Energy 2016;94:213–22.
[3] Omrany H, Ghaffarianhoseini A, Ghaffarianhoseini A, Raahemifar K, Tookey J. Application of passive wall systems for improving the energy efficiency in buildings: a comprehensive review. Renew Sustain Energy Rev 2016;62:1252–69.
[4] Antonopoulos KA, Vrachopoulos M, Tzivanidis C. Experimental evaluation of energy savings in air-conditioning using metal ceiling panels. Appl Therm Eng 1998;18:1129–38.
[5] Kravvaritis ED, Antonopoulos KA, Tzivanidis C, Bellos E. Solar energy management using phase change materials passive systems in the Athens area buildings. Int J Mech Syst Eng 2015;1:102.
[6] Thiele AM, Jamet A, Sant G, Pilon L. Annual energy analysis of concrete containing phase change materials for building envelopes. Energy Convers Manage 2015;103:374–86.
[7] Sarbu I, Sebarchievici C. General review of solar-powered closed sorption refrigeration systems. Energy Convers Manage 2015;105:403–22.
[8] Bellos E, Tzivanidis C, Korres D, Antonopoulos KA. Thermal analysis of a flat plate collector with Solidworks and determination of convection heat coefficient between water and absorber. In: ECOS conference 2015, Pau, France.
[9] Bellos E, Tzivanidis C, Antonopoulos KA. Thermal performance of a direct-flow coaxial evacuated tube with solidworks flow simulation. In: 6th International conference on "experiments/process/system modelling/simulation/optimization, Athens, 8–11 July, 2015.
[10] Tzivanidis C, Bellos E. Parametric analysis of a solar refrigeration system with parabolic trough collectors (PTC). In: Conference MRE 2013, July 2013, Athens.
[11] Fong KF, Lee CK, Chow CK, Yuen SY. Simulation-optimization of solar-thermal refrigeration systems for office use in subtropical Hong Kong. Energy 2011;36:6298–307.
[12] Gunhan T, Ekren O, Demir V, Hepbasli A, Erek A, Sahin AS. Experimental exergetic performance evaluation of a novel solar assisted LiCl–H_2O absorption cooling system. Energy Build 2014;68A:138–46.
[13] Parham K, Atikol U, Yari M, Agboola OP. Evaluation and optimization of single stage absorption chiller using (LiCl + H_2O) as the working pair. Advances in mechanical engineering 2013.
[14] She X, Yin Y, Xu M, Zhang X. A novel low-grade heat-driven absorption refrigeration system with LiCl–H_2O and LiBr–H_2O working pairs. Int J Refrig 2015;58:219–34.
[15] Saleh A, Mosa M. Optimization study of a single-effect water–lithium bromide absorption refrigeration system powered by flat-plate collector in hot regions. Energy Convers Manage 2014;87:29–36.
[16] Beausoleil-Morrison I, Johnson G, Kemery BP. The experimental characterization of a lithium bromide–water absorption chiller and the development of a calibrated model. Sol Energy 2015;122:368–81.
[17] Bellos E, Tzivanidis C, Antonopoulos KA. Comparison of two solar driven absorption chillers for air-conditioning in Greece. In: 6th international conference on "experiments/process/system modelling/simulation/optimization" 6th IC-EpsMsO, Athens, 8–11 July, 2015.
[18] Bellos E, Tzivanidis C, Antonopoulos KA. Exergetic, energetic and financial evaluation of a solar driven absorption cooling system with various collector types. Appl Therm Eng 2016;102:749–59.
[19] Patek J, Klomfar J. Thermodynamic properties of the LiCl-H_2O system at vapor-liquid equilibrium from 273 K to 400 K. Int J Refrig 2008;31(2):287–303.
[20] Li D, Zeng D, Han H, Guo L, Yin X, Yao Y. Phase diagrams and thermochemical modeling of salt lake brine systems. I. LiCl + H_2O system. Calphad 2015;51:1–12.
[21] Kilic M, Kaynakli O. Second law-based thermodynamic analysis of water-lithium bromide absorption refrigeration system. Energy 2007:321505–12.
[22] Gogoi TK, Konwar D. Exergy analysis of a H_2O–LiCl absorption refrigeration system with operating temperatures estimated through inverse analysis. Energy Convers Manage 2016;110:436–47.
[23] Kalogirou S. Solar energy engineering. In: Kalogirou Soteris A, editor. Boston: Academic Press; 2009.
[24] Tsalikis G, Martinopoulos G. Solar energy systems potential for nearly net zero energy residential buildings. Sol Energy 2015;115:743–56.
[25] Borge D, Colmenar A, Castro M, Martín S, Sancristobal E. Exergy efficiency analysis in buildings climatized with LiCl–H_2O solar cooling systems that use swimming pools as heat sinks. Energy Build 2011;43:3161–72.
[26] Balaras CA, Grossman G, Henning H-M, Ferreira CAI, Podesser E, Wang L, et al. Solar air conditioning in Europe – an overview. Renew Sustain Energy Rev 2007;11(2):299–314.